

Directional Symmetry Breaking of Spherical Active Colloids by Magnetoviscous Coupling

Ziyang Zhou,¹ Takuya Kobayashi,^{1,2} Keita Saito,³ Masato Ito,¹ Kohei Yoshinaga,⁴ Yasutaka Iwashita,⁵ Kazusa Beppu,^{1,*} and Yusuke T. Maeda^{1,†}

¹*Department of Chemical Engineering, Kyoto University, Kyoto 615-8510, Japan*

²*Department of Chemical Engineering, Stanford University, Stanford, CA 94305, USA*

³*RIKEN Center for Emergent Matter Science, 2-1 Hirosawa, Wako, Saitama 351-0198, Japan*

⁴*Department of Chemistry, Graduate School of Science, Kyoto University, Kyoto 606-8502, Japan*

⁵*Department of Physics, School of Science, Kyoto Sangyo University, Kyoto 603-8555, Japan*

(Dated: May 27, 2026)

Harnessing active matter requires strategies that break the directional symmetry of self-propelled motion without altering the propulsion mechanism itself. Here, we show that magnetically inert spherical active colloids can be steered through the anisotropic viscous response of a ferrofluid under a uniform magnetic field. Self-propelled Janus colloids exhibit robust cross-field motion transverse to the magnetic field, although the applied magnetic field directly controls neither the particles nor their propulsion speed. Quantitative measurements reveal an emergent reorientation torque that grows with propulsion speed and magnetic field strength. A squirmer model in a magnetoviscous medium captures these observations and shows that the torque arises from the coupling between swimmer-generated flow and anisotropic rotational viscosity. Our findings establish a hydrodynamic foundation for converting viscous dissipation into directional symmetry breaking through anisotropic rheology, providing a route to field-controlled material transport by active matter.

A central challenge in active matter is to understand how self-propelled motion is generated and reoriented, because self-propulsion not only governs the collective states of active matter [1–4] but also underlies transport [5–8] and delivery [9, 10] at the microscale. Self-propelled colloidal particles (active colloids) provide a useful class of active matter, as their motion and interactions can be systematically controlled [11–18]. Yet the physical principles that enable robust directional control, particularly in anisotropic fluid media [19–21], remain less understood than those governing self-propulsion.

An open question is whether anisotropic viscous response alone can reorient an active particle and thereby break the directional symmetry of its motion. In theory, the flow field generated by self-propulsion can couple to anisotropic rheology so as to produce a nontrivial torque even for a spherical swimmer, as predicted for a uniaxially aligned liquid-crystalline medium [22]. However, in experiments on conventional liquid-crystalline media, the contribution of this mechanism has not yet been disentangled from other effects, because swimmer trajectories are influenced not only by anisotropic viscosity associated with orientational order [23–29] but also by topological defects [30–33], viscoelasticity [34–36], anchoring [37–39], and confinement [40].

An attractive route to this problem is provided by ferrofluids, which are suspensions of magnetic nanoparticles (MNPs) [41–44]. Under a uniform magnetic field, they acquire a tunable and reversible uniaxial viscous anisotropy through the field-induced response of magnetic nanoparticles [45–48]. With this anisotropy imposed externally and varied systematically, ferrofluids provide a well-controlled framework for probing how self-

generated flows couple to anisotropic viscosity. In addition, the energy input for particle propulsion can be supplied independently of the field that controls the medium rheology, allowing flow-induced reorientation and directional symmetry breaking in anisotropic media to be identified more directly.

In this Letter, we report robust cross-field motion, transverse to the applied uniform magnetic field, of magnetically inert spherical active colloids dispersed in ferrofluids. We show that this reorientation arises from an emergent torque that appears only when the particles are self-propelled and the ferrofluid exhibits a uniaxial viscous anisotropy. A squirmer model, combined with experiment, reveals a general mechanism of directional symmetry breaking by which anisotropic viscosity steers self-propulsive motion through its coupling to surface-slip-driven propulsion.

We used self-propelled Janus colloids with a chromium (Cr)-coated hemisphere as active colloids, with a diameter of 3.6 μm , dispersed at a density of 0.67 ± 0.15 particles/ $1000 \mu\text{m}^2$. Self-propulsion via induced charge electrophoresis (ICEP) [49–51] was driven by an AC electric field E with a fixed frequency of 2 kHz applied along the z direction through ITO glass electrodes (Fig. 1(a)). The swimming direction of each particle is denoted by θ_v , while the polarity angle θ_p is defined by image analysis of the polarity axis set by the Cr-coated hemisphere. We confirmed that θ_p is aligned with the swimming direction θ_v (Fig. S1). The Janus colloids were dispersed either in an aqueous solution or in a dilute ferrofluid (PBG300, Ferrotec) containing sterically stabilized iron-oxide MNPs at a volume fraction of $\Phi = 0.12\%v/v$. We applied a uniform magnetic field along the y axis using

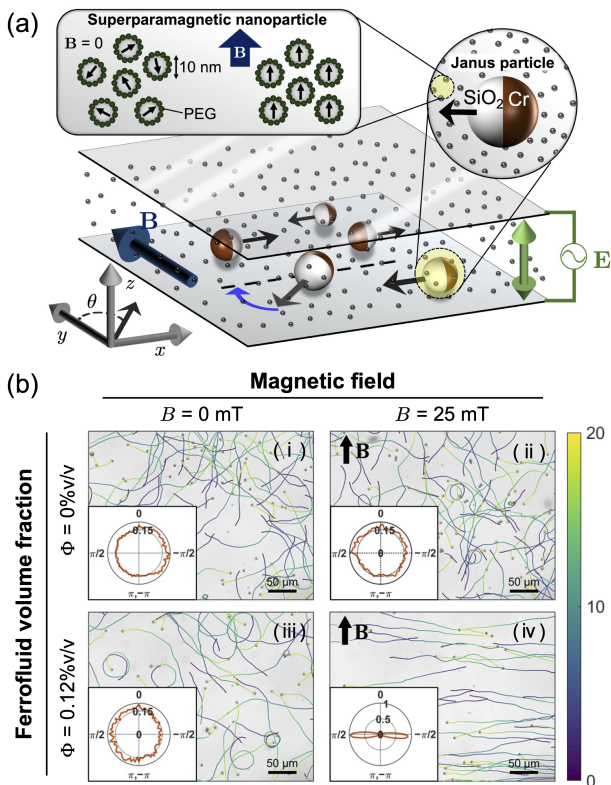


FIG. 1. (a) The experimental setup. The magnetic field is applied along the y direction ($\theta = 0$). (b) Magnetic-field and ferrofluid dependence of the swimming direction. Trajectories of Janus colloids are color-coded. Cross-field motion ($\theta = \pm\pi/2$) is observed only in the ferrofluid with $\Phi = 0.12\%$ under an applied magnetic field, corresponding to condition (iv). Scale bars: $50\ \mu\text{m}$. Inset: Probability distribution of the swimming directions.

a pair of horizontally aligned electromagnets, defining $\theta = 0$ along the axis of the magnetic field (Fig. 1(a)). The magnetic flux density is $\mathbf{B} = B\mathbf{e}_y$, where \mathbf{e}_y denotes the unit vector along the y direction.

Fig. 1(b) establishes the minimal conditions required for field-controlled reorientation of active colloids. In an aqueous solution, the swimming direction θ_v is isotropically distributed both without and with an applied magnetic field (Fig. 1(b)-(i) and (ii), respectively, Movie 1), showing that the Janus colloids themselves are magnetically inert under the present conditions. In ferrofluid, the directional distribution likewise remains isotropic in the absence of a magnetic field (Fig. 1(b)-(iii), Movie 1), indicating that MNPs alone do not bias propulsion. Cross-field motion emerges only when self-propelled particles swim in a ferrofluid under an applied magnetic field (Fig. 1(b)-(iv), Movie 1), where the swimming direction becomes strongly biased toward $\theta = \pm\pi/2$.

We confirmed that, in the absence of AC driving, the polarity angle θ_p remains isotropically distributed even

in the ferrofluid under $B = 25\ \text{mT}$ (Fig. S2). Thus, in the absence of self-generated flows, we find no detectable field-induced orientational bias of the Janus colloids under the present conditions. We also confirmed that the propulsion speed is essentially unchanged by either the magnetic field or the addition of MNPs (Figs. S3 and S4). The same cross-field motion is also observed for Au-coated Janus colloids (Fig. S5), further indicating that the effect does not rely on the weak magnetic susceptibility of the Cr coating. The reorientation therefore requires both the ferrofluid and the applied magnetic field, and does not occur when either of them is absent.

To identify the origin of the effective torque responsible for cross-field motion, we examined how the swimming direction depends on propulsion speed, v . We varied the electric field driving ICEP from $E = 0.008\ \text{V}/\mu\text{m}$ to $0.058\ \text{V}/\mu\text{m}$ and thereby tuned the propulsion speed (Fig. S2). Because individual particles exhibit a distribution of velocities even under a fixed electric-field condition, this dependence was evaluated using the ensemble-averaged speed, \bar{v} . Under a magnetic field of $B = 25\ \text{mT}$, particles with a moderate speed ($\bar{v} = 3.6\ \mu\text{m}/\text{s}$) exhibit preferential orientation at $\theta = \pm\pi/2$ with large angular fluctuations (Fig. 2(a,b)). At a faster speed ($\bar{v} = 9.1\ \mu\text{m}/\text{s}$), the cross-field alignment becomes sharply peaked (Fig. 2(a,b)), showing that the stabilization of cross-field alignment depends on self-propulsion.

The sharpening of cross-field alignment with increasing propulsion speed suggests that the reorientation mechanism is coupled to self-propulsion. To quantify this tendency, we define the orientational order parameter

$$S(t) = \langle \cos 2(\theta_v^j(t) - \theta_B) \rangle_j \quad (1)$$

where θ_v^j is the heading angle of the velocity of the j th particle and $\theta_B = 0$ denotes the magnetic-field direction. Here, $S(t) = 0$ corresponds to isotropic motion, whereas $S(t) < 0$ indicates preferential motion transverse to the field. Because cross-field motion is characterized by the persistent directional bias of the ensemble at the steady state, we quantify it using the time-averaged order parameter, $S_0 = \langle S(t) \rangle_t$. Fig. 2(c) shows that particles exhibit $S_0 < 0$ under all applied magnetic fields, while $S_0 = 0$ is observed only at $B = 0$. Moreover, $|S_0|$ increases with both propulsion speed and magnetic field strength, indicating that stronger fields more effectively stabilize motion perpendicular to the field.

Having established cross-field motion under the applied magnetic field, we next examine the reorientation dynamics by measuring the response to the field switching. We probed the reorientation dynamics by switching the magnetic field from $B = 0\ \text{mT}$ to $B = 15\ \text{mT}$ and monitoring the relaxation of S toward its negative steady-state value S_0 . At long times, the relaxation is well captured by a single-exponential form [52],

$$S(t) = S_0 \left(1 - e^{-t/\tau} \right), \quad (2)$$

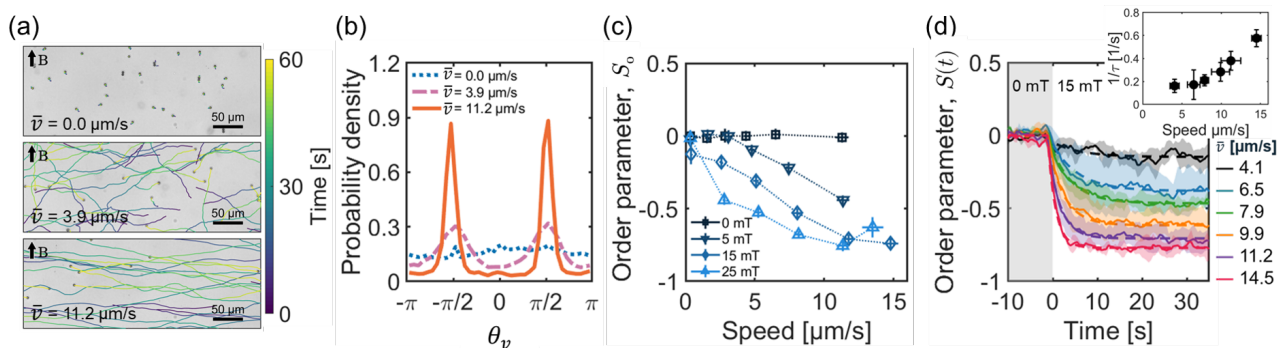


FIG. 2. (a) Speed dependence of cross-field motion of active Janus colloids under the magnetic field $B = 25$ mT. Scale bar: $25 \mu\text{m}$. (b) Probability distributions of the swimming direction θ_v for different propulsion speeds \bar{v} . The probability distributions were calculated from $N = 29846$ ($\bar{v} = 0.0 \mu\text{m/s}$, $E = 0.0 \text{ V}/\mu\text{m}$), 33476 ($\bar{v} = 3.9 \mu\text{m/s}$, $E = 0.033 \text{ V}/\mu\text{m}$) and 17327 ($\bar{v} = 11.2 \mu\text{m/s}$, $E = 0.058 \text{ V}/\mu\text{m}$) tracked particle velocities. (c) Time-averaged orientational order parameter S_0 plotted against the propulsion speed \bar{v} for different magnetic flux densities. (d) Relaxation dynamics of the orientational order parameter $S(t)$ for different values of the speed \bar{v} . Dashed lines are fits to Eq. (2). Inset: The inverse of response time ($1/\tau$) plotted against the propulsion speed \bar{v} .

which defines a reorientation timescale τ (Fig. 2(d)). The inverse response time $1/\tau$ increases with propulsion speed for $\bar{v} \gtrsim 5 \mu\text{m/s}$ (Fig. 2(d), inset). This speed dependence is incompatible with a conventional magnetic torque acting on the particle [47, 48], and instead points to a hydrodynamic torque generated by self-propulsion in the anisotropic medium.

To isolate the hydrodynamic mechanism underlying the field-induced reorientation, we consider a minimal model of a spherical swimmer in a ferrofluid with field-induced viscous anisotropy (Fig. 3(a)). Because the surface slip flow drives Janus colloids transverse to the applied AC electric field [49, 53], the swimming direction lies in the xy plane. We therefore restrict the analysis to this plane, with \mathbf{B} . Following Ref. [54], we model the active colloid of radius a as a squirmer [55] and retain only the first two polar squirming modes, which correspond to self-propulsion and force-dipole flow. The tangential slip velocity profile at the particle surface is prescribed as

$$\mathbf{u}^S(\vartheta) = \frac{3}{2}v_0(\sin\vartheta + \beta\sin\vartheta\cos\vartheta)\mathbf{e}_\vartheta, \quad (3)$$

where v_0 denotes the propulsion speed, ϑ is the polar angle measured from the particle orientation vector \mathbf{p} , and \mathbf{e}_ϑ is the polar unit vector. The squirmer parameter β distinguishes pullers ($\beta > 0$) from pushers ($\beta < 0$) [56]. The far-field flow of active Janus colloids has been reported to exhibit pusher-like characteristics [57]. We focus on the pusher case, $\beta < 0$, throughout the following analysis [58].

Assuming that MNPs remain freely dispersed without chain formation, we describe the ferrofluid stress under a uniform magnetic field by a minimal Shliomis-type con-

stitutive form [41, 44]:

$$\boldsymbol{\sigma} = -p\mathbf{1} + \eta_0\dot{\boldsymbol{\gamma}} + \underbrace{\eta_B[\mathbf{e}_B(\mathbf{e}_B \times \boldsymbol{\omega}) - (\mathbf{e}_B \times \boldsymbol{\omega})\mathbf{e}_B]}_{\boldsymbol{\sigma}_B}. \quad (4)$$

where $\boldsymbol{\omega} \equiv \nabla \times \mathbf{u}$ is vorticity, \mathbf{u} denotes the velocity field of the Stokes flow around the swimmer, and $\mathbf{e}_B \equiv \mathbf{B}/|\mathbf{B}| (= \mathbf{e}_y)$ is the magnetic-field direction. The first term is the isotropic pressure enforcing incompressibility, and the second term is the Newtonian viscous stress with shear rate $\dot{\boldsymbol{\gamma}}$ and viscosity η_0 . The third term represents the field-induced magnetoviscous stress $\boldsymbol{\sigma}_B$, which captures the rotational-viscosity response of the ferrofluid arising from the coupling between the local vorticity $\boldsymbol{\omega}$ and field-aligned MNPs. Its magnitude is set by the magnetoviscous coefficient $\eta_B = \alpha(B)B^2/(4\mu_0)$ where μ_0 is the vacuum permeability and $\alpha(B)$ is the transport coefficient.

To evaluate the torque \mathbf{T} from the anisotropic stress $\boldsymbol{\sigma}_B$, we substitute the Stokes flow around a spherical squirmer into Eq. (4) [52]. The torque is then given by,

$$\mathbf{T} = \int_S \mathbf{r} \times (\boldsymbol{\sigma} \cdot \hat{\mathbf{r}}) dS = \frac{6}{5}\pi\eta_B a^2 \beta v_0 (\mathbf{p} \cdot \mathbf{e}_B) (\mathbf{p} \times \mathbf{e}_B). \quad (5)$$

The resulting orientational dynamics follow directly from torque balance between Eq. (5) and rotational viscous drag. Let $\theta_p = \cos^{-1}(\mathbf{p} \cdot \mathbf{e}_B)$ be the polar angle of the squirmer orientation \mathbf{p} measured from \mathbf{e}_B . The corresponding angular velocity about the z axis is $\boldsymbol{\Omega} = -\dot{\theta}_p \mathbf{e}_z$. The torque balance relation, $\mathbf{T} - 8\pi\eta_0 a^3 \boldsymbol{\Omega} = 0$, yields

$$\dot{\theta}_p = \Gamma \sin(2\theta_p), \quad \Gamma = -\frac{3}{40} \frac{\beta v_0 \eta_B}{a \eta_0}. \quad (6)$$

where Γ denotes the reorientation rate. For a pusher, this equation predicts stable states at $\theta_p = \pm\pi/2$ (Fig. 3(b)),

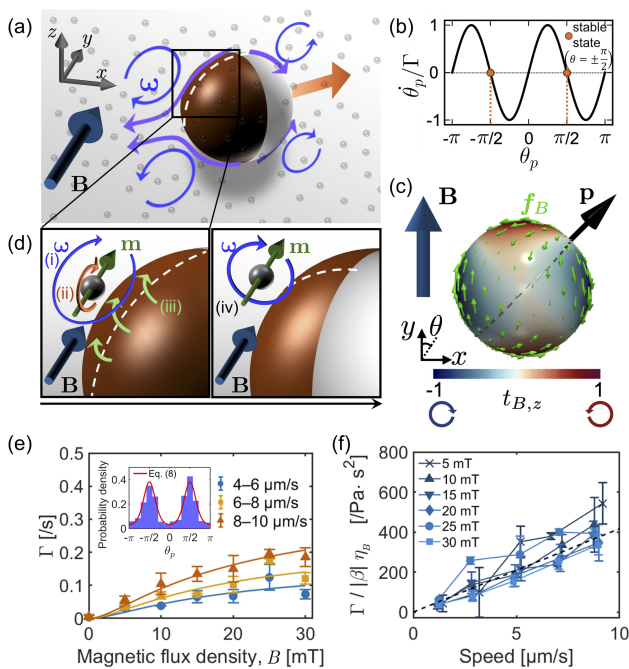


FIG. 3. (a) Schematic of a pusher-type active colloid in a ferrofluid under a uniform magnetic field \mathbf{B} , showing the surface-slip flow and associated vorticity $\boldsymbol{\omega}$. (b) Angular dependence of the reorientation dynamics $\dot{\theta}_p/\Gamma$, with stable states at $\theta_p = \pm\pi/2$. (c) Torque density $t_{B,z}$ on a pusher arising from the stress $\boldsymbol{\sigma}_B$. Green arrows on the particle surface indicate the force density \mathbf{f}_B . (d) The mechanism of cross-field alignment. (i) Pusher-induced vorticity, $\boldsymbol{\omega}$. (ii) Flow-induced rotation of MNP magnetic moment \mathbf{m} , counteracted by alignment with \mathbf{B} . (iii) Magnetoviscous stress: asymmetric surface traction (green arrows). (iv) Stable cross-field alignment when the vorticity in the fore-aft plane aligns with the field. (e) The reorientation rate Γ plotted against B . Particles were grouped into the propulsion-speed ranges. Solid lines are fits to Γ in Eq. (6). Inset: Probability density of θ_p under $B = 30$ mT and $v = 4\text{--}6$ $\mu\text{m/s}$. Red line is fit to Eq. (8). (f) $\Gamma/|\beta|\eta_B$ against \bar{v} shown for $B = 5$ to 30 mT. The data collapse onto a single master curve (the dashed line).

showing that the torque rotates the particle axis toward an orientation perpendicular to the applied field.

It is worth noting that the ICEP slip flow of Janus colloids differs from the axisymmetric squirmer slip [57]. To test whether this difference affects the reorientation dynamics, we performed direct numerical simulations of spherical swimmers [52, 59–63] separately using the ICEP slip profile and the squirmer slip profile, without relying on the analytical approximations used in anisotropic stress calculation. For both slip profiles in a fluid with uniaxial magnetoviscous anisotropy, the simulations reproduced cross-field motion and agreed with the analytical solution of the squirmer model (Fig. S6). This agreement with the analytical squirmer solution supports the squirmer model as an effective hydrodynamic description for the observed reorientation dynamics.

To further reveal the origin of the reorientation torque, we illustrate the surface force density \mathbf{f}_B and the resulting torque density \mathbf{t}_B arising from the field-induced stress $\boldsymbol{\sigma}_B$ (Fig. 3(c)),

$$\mathbf{f}_B = \boldsymbol{\sigma}_B|_{r=a} \cdot \hat{\mathbf{r}}, \quad \mathbf{t}_B = a \hat{\mathbf{r}} \times \mathbf{f}_B, \quad (7)$$

where $\hat{\mathbf{r}}$ is the radial unit vector. The region with negative $t_{B,z}$ dominates over the positive one, driving pushers toward perpendicular to the applied field (Fig. 3(c)).

The mechanism of cross-field alignment is summarized as follows (Fig. 3(d)): (i) A pusher generates vorticity $\boldsymbol{\omega}$ in its near field. (ii) When $\boldsymbol{\omega}$ is not aligned with the magnetic field \mathbf{B} , the local rotation tends to misalign the magnetic moment \mathbf{m} of a dispersed MNP with respect to \mathbf{B} , while the magnetic torque $\mathbf{m} \times \mathbf{B}$ tends to counteract this flow-induced misalignment. (iii) This competition generates a magnetoviscous stress in the surrounding ferrofluid, which produces an asymmetric surface traction on the swimmer (green arrows) and thereby a net reorienting torque. (iv) Cross-field alignment arises when this net torque vanishes.

Eq. (6) indicates that the reorientation rate Γ increases with the propulsion speed and the field-dependent magnetoviscosity. We next apply a Langevin-type statistical analysis of the orientation dynamics to evaluate Γ from the experimental data [52]. The probability distribution of particle orientation is given by

$$P(\theta_p) = P_0 \exp\left(-\frac{\Gamma}{D_\theta} \cos^2 \theta_p\right), \quad (8)$$

where P_0 is a normalization constant and D_θ is the rotational diffusion coefficient. Using independently measured $D_\theta = 0.051 \text{ s}^{-1}$ (Fig. S7), fitting Eq. (8) to the measured $P(\theta_p)$ directly yields Γ .

The measured $P(\theta_p)$ agrees well with Eq. (8) (Fig. 3(e) inset). The experimentally obtained Γ , plotted separately for particles swimming at slow, moderate, and fast speeds, increases with B in all cases (blue, yellow, red in Fig. 3(e), respectively). The data are well described by Eq. (6) using the field-dependent magnetoviscosity η_B (see End Matter for details). The gradual saturation of Γ with B reflect the corresponding field dependence of the magnetoviscous response of the ferrofluid.

Eq. (6) also predicts that $\frac{\Gamma}{|\beta|\eta_B}$ scales linearly with propulsion speed v_0 , with a slope of $\frac{3}{40a\eta_0}$. Using the values of $|\beta|\eta_B$ extracted from Fig. 3(e), we rescaled Γ and plotted it against \bar{v} . The data for all magnetic field strengths collapse onto a linear master curve (Fig. 3(f)), providing further support for the emergent coupling between self-propulsion and anisotropic viscosity.

The aligning mechanism revealed here is structurally related to an emergent torque theoretically predicted for swimmers in liquid-crystalline media [22]: in both cases, swimmer-generated vorticity couples to an anisotropic

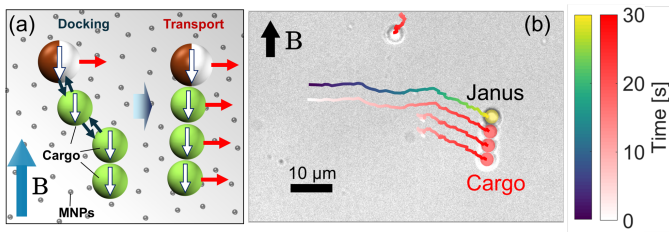


FIG. 4. (a, b) Cargo particle transport. White arrows and blue arrows in (a) represent the induced magnetic moment and the dipolar attraction, respectively. (b) The active Janus colloid is marked in yellow, and the PS cargo particles are in red. $\Phi = 0.24\%$, $B = 30$ mT, $E = 0.033$ V/ μm . The density of cargo particles is 5.0 particles/ $1000 \mu\text{m}^2$. Scale bar: $10 \mu\text{m}$.

response of the host medium to generate a reorientation torque. The distinction is that the effective rotational viscosity is positive in ferrofluids but negative in the liquid-crystal model [64, 65], which reverses the stable orientation from perpendicular to parallel alignment. This correspondence suggests that the coupling between swimmer-generated flow and anisotropic rotational viscosity is a generic route to steering self-propulsive motion across microscopically distinct anisotropic media.

An important implication of our finding is its potential for cargo loading and directed transport. To demonstrate this capability, we dispersed passive polystyrene (PS) microspheres with a diameter of $3.0 \mu\text{m}$ in a ferrofluid containing active Janus colloids. Under an applied magnetic field, both active and passive particles behave as nonmagnetic voids in the ferrofluid and acquire induced magnetic moments antiparallel to the field [66]. The resulting dipolar attraction drives the formation of particle clusters aligned along the field direction. A Janus particle can capture Brownian PS particles to form composite Janus–cargo assemblies (Fig. 4(a)). These assemblies subsequently undergo cross-field motion, thereby achieving cargo transport without requiring magnetic or shape anisotropy of the cargo (Fig. 4(b), Movie 3).

In this work, we have demonstrated robust cross-field motion of magnetically inert spherical active colloids in ferrofluids under a uniform magnetic field. Ferrofluids allow externally imposed anisotropic viscosity to be separated from topological defects, elastic effects, and confinement. This separation enables experimental isolation of the hydrodynamic reorientation torque predicted for anisotropic media. More broadly, our results establish anisotropic rheology as a controllable physical variable for converting viscous dissipation into directional symmetry breaking of active motion, with dilute dispersions of MNPs providing a minimal experimental realization. The rapid response of ferrofluids further enables reversible control of cross-field alignment within $\tau \sim 1.6$ s (Fig. S8, Movie 3), and may provide access to collec-

tive motion and pattern formation associated with time-dependent responses and odd viscosity [67, 68].

Acknowledgements.— We would like to thank T. Sakaue and D. Nishiguchi for discussions. This work was supported by Grant-in-Aid for Scientific Research (B) (23K25841), Grant-in-Aid for Transformative Research Areas(B)(26K00015), Grant-in-Aid for Research Activity Start-up (25K23356), Hosokawa Powder Technology Foundation, The Information Center of Particle Technology, JST FOREST Grant (JPMJFR2239), JSPS Core-to-Core Program “Advanced core-to-core network for the physics of self-organizing active matter” (JPJSCCA20230002).

Data availability statement.— The data that support the findings of this study will be publicly available upon publication.

Remark.— Z.Z. and T.K. equally contributed to this work.

* kazusa.beppu@cheme.kyoto-u.ac.jp

† maeda@cheme.kyoto-u.ac.jp

- [1] M. C. Marchetti, J.-F. Joanny, S. Ramaswamy, T. B. Liverpool, J. Prost, M. Rao, and R. A. Simha, *Rev. Mod. Phys.* **85**, 1143 (2013).
- [2] S. Michelin, *Ann. Rev. Fluid Mech.* **55**, 77 (2023).
- [3] J. Elgeti, R. G. Winkler, and G. Gompper, *Rep. Prog. Phys.* **78**, 056601 (2015).
- [4] S. E. Spagnolie and P. T. Underhill, *Ann. Rev. Cond. Matt. Phys.* **14**, 381 (2023).
- [5] A. M. Boymelgreen, T. Balli, T. Miloh, and G. Yossifon, *Nat. Commun.* **9**, 760 (2018).
- [6] A. F. Demirörs, M. T. Akan, E. Poloni, and A. R. Studart, *Soft Matter* **14**, 4741 (2018).
- [7] M. Ussia, M. Urso, C. M. Oral, X. Peng, and M. Pumera, *ACS Nano* **18**, 13171 (2024).
- [8] S.-J. Song, J. Kim, R. Gabor, R. Zboril, and M. Pumera, *ACS Nano* **19**, 27259 (2025).
- [9] A. Ghosh, W. Xu, N. Gupta, and D. H. Gracias, *Nano Today* **31**, 100836 (2020).
- [10] W. Gao and J. Wang, *Nanoscale* **6**, 10486 (2014).
- [11] J. Palacci, S. Sacanna, A. P. Steinberg, D. J. Pine, and P. M. Chaikin, *Science* **339**, 936 (2013).
- [12] J. Simmchen, J. Katuri, W. E. Uspal, M. N. Popescu, M. Tasinkevych, and S. Sánchez, *Nat. Commun.* **7**, 10598 (2016).
- [13] C. Bechinger, R. Di Leonardo, H. Löwen, C. Reichhardt, G. Volpe, and G. Volpe, *Rev. Mod. Phys.* **88**, 045006 (2016).
- [14] B. Liebchen and H. Lowen, *Acc. Chem. Res.* **51**, 2982 (2018).
- [15] J. Katuri, W. E. Uspal, J. Simmchen, A. Miguel-López, and S. Sánchez, *Sci. Adv.* **4**, eaao1755 (2018).
- [16] M. N. van der Linden, L. C. Alexander, D. G. A. L. Aarts, and O. Dauchot, *Phys. Rev. Lett.* **123**, 098001 (2019).
- [17] S. Auschra, A. Bregulla, K. Kroy, and F. Cichos, *The European Physical Journal E* **44**, 90 (2021).
- [18] J. Zhang, R. Alert, J. Yan, N. S. Wingreen, and S. Granick, *Nat. Phys.* **17**, 961 (2021).

- [19] O. D. Lavrentovich, *Curr. Opin. Colloid Interface Sci.* **21**, 97 (2016).
- [20] I. S. Aranson, *Acc. Chem. Res.* **51**, 3023 (2018).
- [21] E. Bukusoglu, M. Bedolla Pantoja, P. C. Mushenheim, X. Wang, and N. L. Abbott, *Ann. Rev. Chem. Biomol. Eng.* **7**, 163 (2016).
- [22] J. S. Lintuvuori, A. Würger, and K. Stratford, *Phys. Rev. Lett.* **119**, 068001 (2017).
- [23] S. Zhou, A. Sokolov, O. D. Lavrentovich, and I. S. Aranson, *Biophys. J.* **106**, 420a (2014).
- [24] P. Guillamat, J. Ignés-Mullol, and F. Sagués, *Proc. Natl. Acad. Sci. USA* **113**, 5498 (2016).
- [25] S. Zhou, O. Tovkach, D. Golovaty, A. Sokolov, I. S. Aranson, and O. D. Lavrentovich, *New J. Phys.* **19**, 055006 (2017).
- [26] M. M. Genkin, A. Sokolov, O. D. Lavrentovich, and I. S. Aranson, *Phys. Rev. X* **7**, 011029 (2017).
- [27] T. Turiv, R. Koizumi, K. Thijssen, M. M. Genkin, H. Yu, C. Peng, Q.-H. Wei, J. M. Yeomans, I. S. Aranson, A. Doostmohammadi, *et al.*, *Nat. Phys.* **16**, 481 (2020).
- [28] R. Koizumi, T. Turiv, M. M. Genkin, R. J. Lastowski, H. Yu, I. Chaganava, Q.-H. Wei, I. S. Aranson, and O. D. Lavrentovich, *Phys. Rev. Res.* **2**, 033060 (2020).
- [29] L.-L. Ma, C. Liu, S.-B. Wu, P. Chen, Q.-M. Chen, J.-X. Qian, S.-J. Ge, Y.-H. Wu, W. Hu, and Y.-Q. Lu, *Sci. Adv.* **7**, eabh3505 (2021).
- [30] C. Peng, T. Turiv, Y. Guo, Q.-H. Wei, and O. D. Lavrentovich, *Science* **354**, 882 (2016).
- [31] M. Rajabi, H. Baza, T. Turiv, and O. D. Lavrentovich, *Nat. Phys.* **17**, 260 (2021).
- [32] M. Lesniewska, N. Mottram, and O. Henrich, *Soft Matter* **18**, 6942 (2022).
- [33] D. K. Sahu and S. Dhara, *Soft Matter* **18**, 1819 (2022).
- [34] I. I. Smalyukh, J. Butler, J. D. ShROUT, M. R. Parsek, and G. C. Wong, *Phys. Rev. E* **78**, 030701 (2008).
- [35] H. Chi, A. Gavrikov, L. Berlyand, and I. S. Aranson, *Commun. Phys.* **5**, 274 (2022).
- [36] H. Baza, F. Chen, T. Turiv, S. V. Shiyonovskii, and O. D. Lavrentovich, *Soft Matter* **22**, 1297 (2015).
- [37] H. Chi, M. Potomkin, L. Zhang, L. Berlyand, and I. S. Aranson, *Commun. Phys.* **3**, 162 (2020).
- [38] D. K. Sahu, S. Kole, S. Ramaswamy, and S. Dhara, *Phys. Rev. Res.* **2**, 032009 (2020).
- [39] D. G. Sudha, H. Baza, D. P. Rivas, S. Das, O. D. Lavrentovich, and L. S. Hirst, *Phys. Rev. E* **110**, 054704 (2024).
- [40] S. Mandal, T. J. Mason, A. C. Croft, and M. G. Mazza, *Phys. Rev. Lett.* **134**, 128302 (2025).
- [41] M. I. Shliomis, *Soviet Physics Uspekhi* **17**, 153 (1974).
- [42] S. Odenbach, *Inter. J. Modern Phys. B* **14**, 1615 (2000).
- [43] S. Odenbach, ed., *Colloidal Magnetic Fluids: Basics, Development and Application of Ferrofluids*, Lecture Notes in Physics, Vol. 763 (Springer Berlin Heidelberg, 2009).
- [44] S. Mahle, P. Ilg, and M. Liu, *Phys. Rev. E* **77**, 016305 (2008).
- [45] T. Cherian, F. Sohrabi, C. Rigoni, O. Ikkala, and J. V. Timonen, *Sci. Adv.* **7**, eabi8990 (2021).
- [46] V. Socoliuc, M. Avdeev, V. Kuncser, R. Turcu, E. Tombác, and L. Vékás, *Nanoscale* **14**, 4786 (2022).
- [47] S. Wang, Y. Chen, X. Zhou, L. Lei, Z. H. Shah, G. Lin, and Y. Gao, *Langmuir* **37**, 1429 (2021).
- [48] K. Beppu and J. Timonen, *Commun. Phys.* **7**, 216 (2024).
- [49] M. Z. Bazant and T. M. Squires, *Phys. Rev. Lett.* **92**, 066101 (2004).
- [50] T. M. Squires and M. Z. Bazant, *J. Fluid Mech.* **509**, 217 (2004).
- [51] S. Gangwal, O. J. Cayre, M. Z. Bazant, and O. D. Velev, *Phys. Rev. Lett.* **100**, 058302 (2008).
- [52] See Supplemental Material at <http://link.aps.org/> for additional theoretical details and experimental analysis..
- [53] T. M. Squires and M. Z. Bazant, *Journal of Fluid Mechanics* **560**, 65 (2006).
- [54] Z. Shen, A. Würger, and J. S. Lintuvuori, *Eur. Phys. J. E Soft Matter* **41**, 39 (2018).
- [55] J. R. Blake, *J. Fluid Mech.* **46**, 199 (1971).
- [56] T. Ishikawa, M. P. Simmonds, and T. J. Pedley, *J. Fluid Mech.* **568**, 119 (2006).
- [57] D. Nishiguchi and M. Sano, *Phys. Rev. E* **92**, 052309 (2015).
- [58] C. Peng, I. Lazo, S. V. Shiyonovskii, and O. D. Lavrentovich, *Phys. Rev. E* **90**, 051002 (2014).
- [59] Y. Nakayama and R. Yamamoto, *Phys. Rev. E* **71**, 036707 (2005).
- [60] J. J. Molina, Y. Nakayama, and R. Yamamoto, *Soft Matter* **9**, 4923 (2013).
- [61] R. Yamamoto, J. J. Molina, and Y. Nakayama, *Soft Matter* **17**, 4226 (2021).
- [62] T. Kobayashi, G. Jung, Y. Matsuoka, Y. Nakayama, J. J. Molina, and R. Yamamoto, *Soft Matter* **19**, 7109 (2023).
- [63] T. Kobayashi, J. J. Molina, and R. Yamamoto, *Phys. Rev. Res.* **6**, 033304 (2024).
- [64] P.-G. De Gennes and J. Prost, *The physics of liquid crystals*, 83 (Oxford university press, 1993).
- [65] D. Marenduzzo, E. Orlandini, M. Cates, and J. Yeomans, *Phys. Rev. E* **76**, 031921 (2007).
- [66] A. T. Skjeltorp, *Phys. Rev. Lett.* **51**, 2306 (1983).
- [67] T. Markovich and T. C. Lubensky, *Proc. Natl. Acad. Sci. USA* **121**, e2219385121 (2024).
- [68] Y. Hosaka, M. Chatzittofi, R. Golestanian, and A. Vilfan, *Phys. Rev. Res.* **6**, L032044 (2024).
- [69] C. Rigoni, G. Beaune, B. Harnist, F. Sohrabi, and J. V. I. Timonen, *Commun. Mater.* **3**, 26 (2022).
- [70] J. Schindelin, I. Arganda-Carreras, E. Frise, V. Kaynig, M. Longair, T. Pietzsch, S. Preibisch, C. Rueden, S. Saalfeld, B. Schmid, *et al.*, *Nat. Methods* **9**, 676 (2012).
- [71] J.-Y. Tinevez, N. Perry, J. Schindelin, G. M. Hoopes, G. D. Reynolds, E. Laplantine, S. Y. Bednarek, S. L. Shorte, and K. W. Eliceiri, *Methods* **115**, 80 (2017).

End Matter

We clarify the quantitative analysis demonstrated in Figs. 3(e) and (f). This analysis provides the independently determined field dependence of η_B used to test the predicted scaling of the reorientation rate Γ .

Magnetic field dependence of η_B and Γ — The mass magnetization $M^*(B)$ of ferrofluids is well described by the Fröhlich–Kennelly model [69]. Writing the volume magnetization as $M(B) = \rho_f M^*(B)$, we use

$$M^*(H) = \frac{M(H)}{\rho_f} = \frac{\chi_0 H M_s}{\rho_f (\chi_0 H + M_s)}, \quad H = \frac{B}{\mu_0}, \quad (9)$$

where ρ_f is the mass density of the ferrofluid, M_s is the saturation magnetization, and χ_0 is the initial magnetic susceptibility. μ_0 is the vacuum permeability.

We define the field-dependent differential susceptibility by

$$\chi_f(B) \equiv \frac{\partial M}{\partial H}. \quad (10)$$

Using Eq. (9), this becomes

$$\chi_f(B) = \frac{\chi_0}{\left(1 + \frac{B\chi_0}{\mu_0 M_s}\right)^2}. \quad (11)$$

For a monodisperse ferrofluid where MNPs remain freely dispersed without chain formation, the transport coefficient α is written as

$$\alpha(B) = \frac{\tau_f \chi_f(B)}{[1 + \chi_f(B)]^2}, \quad (12)$$

where τ_f denotes the magnetic relaxation time of the free particles. Substituting Eq. (11) into Eq. (12) yields

$$\alpha(B) = \tau_f \chi_0 \frac{\left(1 + \frac{B\chi_0}{\mu_0 M_s}\right)^2}{\left[\left(1 + \frac{B\chi_0}{\mu_0 M_s}\right)^2 + \chi_0\right]^2}. \quad (13)$$

Using $\eta_B = \alpha(B)B^2/(4\mu_0)$ and Eq. (6) in the main text, the reorientation rate Γ is written as

$$\Gamma = -\frac{3\beta v_0}{160 a \mu_0 \eta_0} \alpha(B) B^2. \quad (14)$$

Combining Eq. (13) and Eq. (14) gives the explicit expression

$$\Gamma = -\frac{3\beta v_0 \tau_f \chi_0}{160 a \mu_0 \eta_0} \frac{B^2 \left(1 + \frac{B\chi_0}{\mu_0 M_s}\right)^2}{\left[\left(1 + \frac{B\chi_0}{\mu_0 M_s}\right)^2 + \chi_0\right]^2} \quad (15)$$

which is used to describe the magnetic-field dependence of Γ for particle groups with a given mean propulsion speed v_0 . In the analysis of Fig. 3(e), the viscous coefficient $\eta_0 = 1.0$ mPa s, the particle radius $a = 1.6$ μm , $\mu_0 = 4\pi \times 10^{-7}$ H/m, and the magnetometry-determined parameters χ_0 and M_s introduced in the following section are treated as fixed parameters, whereas $\beta\tau_f$ is taken as the fitting parameter.

Magnetometry-based evaluation of χ_0 and M_s — We performed magnetometry of the diluted PBG300 ferrofluid and used the resulting magnetization curve to determine the saturation magnetization M_s and the initial magnetic susceptibility χ_0 . In our monodisperse-ferrofluid description in Eq. (13), $\alpha(B)$ is directly related to the magnetoviscous coefficient η_B and is therefore an important quantity for evaluating the master curve in

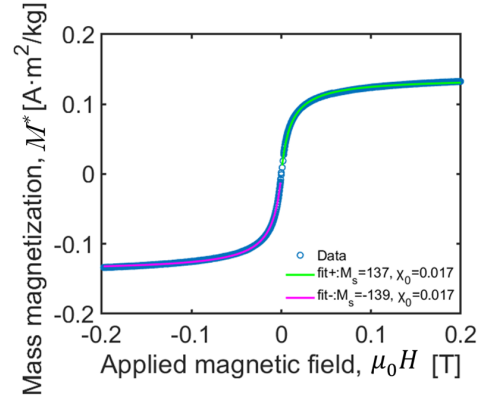


FIG. 5. Mass magnetization of PBG300 ferrofluids. The positive direction is defined as the magnetic field \mathbf{B} parallel to the measurement axis (\mathbf{e}_y), while the negative direction corresponds to the antiparallel field. The fitting curves (green and red) are obtained using Eq. (S10) with parameters $M_s = 137$ and $\chi_0 = 0.017$ for positive values, and $M_s = 139$ and $\chi_0 = 0.017$ for negative values.

Fig. 3(f). Because $\alpha(B)$ is expressed as a function of the magnetic susceptibility χ_f , the parameters that determine its functional form, namely χ_0 and M_s , can be estimated from magnetometry-based measurements of the mass magnetization M^* .

Magnetization measurements were performed at room temperature using a vibrating sample magnetometer (VSM-5, Toei Industry Co., Ltd.) on a diluted PBG300 ferrofluid with a nanoparticle volume fraction of $\Phi = 0.12\%$ v/v. The magnetic field was swept quasi-statically over the range from -0.2 T to $+0.2$ T. A volume of 200 μL of the diluted ferrofluid was loaded into a plastic assay tube attached to a quartz rod and sealed to prevent evaporation.

The measured mass magnetization M^* is shown in Fig. 5. Fitting Eq. (9) to the positive-field sweep yields $M_s = 137$ A m^{-1} and $\chi_0 = 0.017$, whereas fitting to the negative-field sweep gives $M_s = 139$ A m^{-1} and $\chi_0 = 0.017$. The agreement confirms that the Fröhlich-Kennelly form captures the magnetic response of the dilute ferrofluid in the present regime [69]. These independently estimated parameters were further used as experimentally determined material constants when comparing the magnetic-field dependence of the reorientation rate Γ , given by Eq. (14), with the data in Fig. 3(e).

Evaluation of a linear master curve using Eq. (15) — We experimentally determined the reorientation rate Γ by combining the angular distribution of the particle polarity vector with an independent measurement of the rotational diffusion coefficient. In Fig. 3(e), Γ is plotted as a function of the magnetic field B for particle groups with different mean velocities, and its field dependence is verified by fitting the data to Eq. (6), or more com-

pletely to Eq. (15). In this analysis, the product $\beta\tau_f$ is treated as the only remaining fitting parameter. Notably, the obtained values of $\beta\tau_f$ vary slightly with propulsive speed, but remain within the range from -3.58×10^{-3} s to -4.14×10^{-3} s. Although the magnitude of β is not measured independently, the sign of the observed stable orientation selects the pusher-like branch.

Together with Eq. (15) and Eq. (6), the evaluation of $\beta\tau_f$ allows us to determine $|\beta|\eta_B$ for each mean propulsive speed \bar{v} (corresponding to v_0 in the squirmer model). Although Γ depends on both the magnetic field strength B and the propulsive speed v_0 , rescaling the independently measured Γ by these values of $|\beta|\eta_B$ removes the magnetic-field dependence and yields a linear master curve that retains only the speed dependence. As shown in Fig. 3(f), the resulting dependence on the propulsive speed is linear, in agreement with the extended squirmer model.

Supplemental Material

MATERIALS AND METHODS

Preparation of Janus colloidal particles

The Janus colloids were fabricated as follows. A monolayer of silica particles with a diameter of 3.6 μm (Hypercica, UEXC) was first formed at an air-water interface and then transferred onto a glass slide. For chromium (Cr)-coated Janus colloids, one surface of the monolayer was first coated with a 20 nm-thick Cr layer using an electron-beam deposition system (EB-20, Vacuum Device). Subsequently, a 5 nm-thick SiO_2 layer was deposited on the Cr layer using a sputtering system (nano PVD-S10A, Moorfield Nanotechnology). For gold (Au)-coated Janus colloids, a 3 nm-thick Cr layer was first coated and then followed by a 17 nm-thick Au layer using a thermal deposition system (VPC-260F, ULVAC KIKO). After the deposition, the monolayer on the glass slide was immersed in deionized (DI) water, and the Janus colloids were removed from the glass slide by sonication. The Janus colloids were washed with DI water and isopropyl alcohol. The prepared particles were used as a suspension with a particle density of 0.67 ± 0.15 particles/ $1000 \mu\text{m}^2$, containing 0.5% hydrophilic non-ionic surfactant Pluronic F-127 (P2443, Sigma-Aldrich).

Microscopy

An inverted fluorescence microscope (IX73, Evident) equipped with a CMOS camera (Neo 5.5, Andor Technology) was used for both phase-contrast and fluorescence imaging with 20x or 40x objective lenses. Time-lapse recordings of the self-propelled motion of active Janus colloids were acquired at 1-s intervals with Metamorph software (Molecular Devices). The suspension of the active colloids was introduced into a chamber assembled from two indium tin oxide (ITO)-coated cover slips (18×18 mm, resistivity 15–30 Ω , Alliance Biosystems) separated by a 120 μm -thick double-sided spacer (SecureSeal imaging spacer, Grace Bio-Labs), and an AC voltage was applied through a function generator (maximum output voltage, 10.0 Vpp; AFG-2105, Instek Japan). Before chamber assembly, the ITO-coated cover slips were immersed in a 5.0% Pluronic F-127 surfactant solution at room temperature for 3 hour to prevent nonspecific adhesion of the Janus colloids to the ITO electrode surfaces. Polystyrene particles used for demonstrating Janus-cargo assembly transport were fluorescent microspheres with a diameter of 3.0 μm (POL-17147-5, Polysciences, Inc.). For simultaneous imaging of Janus colloids and fluorescent cargo particles, phase-contrast and fluorescence images were acquired concurrently by combining illumination from two light sources.

Image Processing

Image processing and analysis were performed using MATLAB (MathWorks) and Fiji (open-source software) [70]. Raw microscopy images were preprocessed in MATLAB by binarization and intensity inversion, resulting in images with white particles on a black background. Subsequently, these images were analyzed using the TrackMate plugin [71] in Fiji. Particle detection was performed using the Laplacian of Gaussian (LoG) detector, and particle trajectories were reconstructed using the Kalman tracking algorithm to link detections across frames. This procedure yielded the time-dependent positions of individual particles, which were used for subsequent trajectory-based analysis.

The polarity vector \mathbf{p} of each Janus particle was determined by the phase contrast image obtained with a 100x objective lens. The Cr-coated hemisphere was first detected from the image contrast. We then identified two characteristic points, (1) the geometric center of the spherical particle, obtained from its circular outline, and (2) the centroid of the image intensity, which reflects the black-white contrast between the Cr-coated hemisphere and the SiO_2 hemisphere. The polarity vector \mathbf{p} was defined as the vector from the geometric center to the intensity centroid. The polarity angle θ_p was then defined as the angle of \mathbf{p} measured from the magnetic-field axis.

Ferrofluids and a horizontal uniform magnetic field

We used a biocompatible ferrofluid (PBG300, Ferrotec) containing sterically stabilized iron-oxide magnetic nanoparticles. The viscosity η_0 of the diluted ferrofluid containing 0.5% Pluronic F-127 was measured using a rheometer (MCR 302, Anton Paar) equipped with a cone-and-plate geometry (CP25-1).

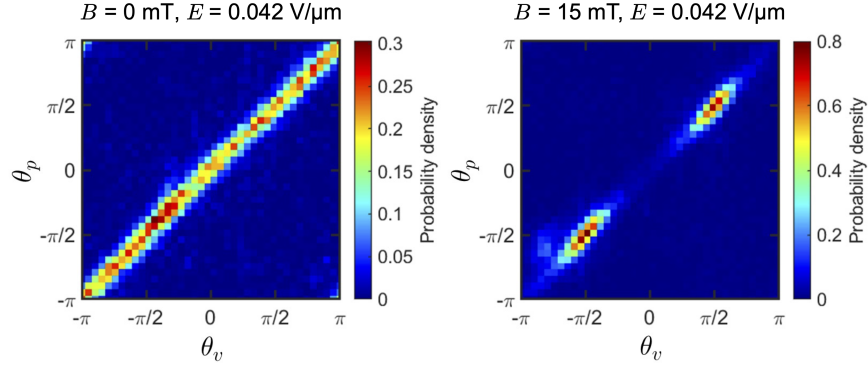


FIG. S1. Linear correspondence between the direction of the velocity vector θ_v and the direction of the polarity vector θ_p of active Janus colloids. The left and right panels correspond to $B = 0$ mT and $B = 25$ mT, respectively.

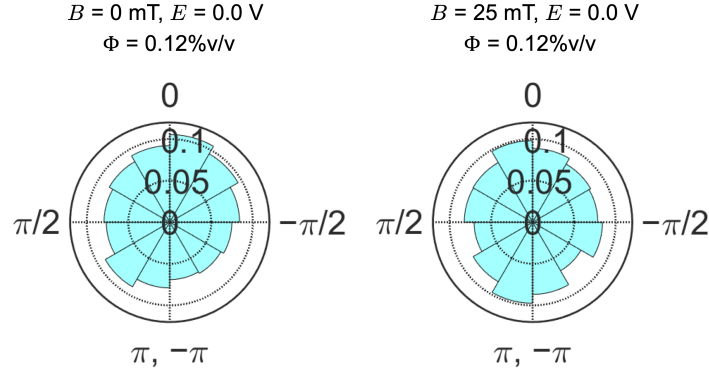


FIG. S2. Distribution of the orientation angle of Janus colloidal particles in a ferrofluid ($\Phi = 0.12\%v/v$) without AC electric-field driving. (Left) No magnetic field, $B = 0$ mT and no electric-field driving, $E = 0.0$ V/ μm . $N = 7564$. (Right) With magnetic field, $B = 25$ mT and no electric-field driving, $E = 0.0$ V/ μm . $N = 8472$.

A uniform horizontal magnetic field was generated using a pair of custom-made electromagnets (TKS-37032, Toei Co., Ltd.), driven by a DC power supply (PWR401ML, KIKUSUI), with the applied current controlled using sequence creation and control software (SD027-PWR-01, KIKUSUI). The field was uniform over a $5\text{ mm} \times 5\text{ mm}$ planar region centered at the sample position. The magnetic field magnitude B was determined from the manufacturer-provided field-current calibration, $B = 68.95 I - 0.001935$ (mT), where I is the applied current (in A).

THE EFFECT OF A MAGNETIC FIELD ON PARTICLE ORIENTATION IN THE ABSENCE OF AN ELECTRIC FIELD

To test whether a magnetic field alone can bias the particle orientation, we quantified the orientation-angle distribution of Cr-coated Janus colloids in a ferrofluid ($\Phi = 0.12\%v/v$) without AC electric-field driving. Figure S2 shows that, within the angular range measurable from side-oriented particles, the particles exhibit no orientational preference either in the absence of a magnetic field ($B = 0$ mT, $E = 0$ V/ μm) or under a uniform magnetic field ($B = 25$ mT, $E = 0$ V/ μm). This confirms that the observed cross-field motion does not originate from passive magnetic alignment of the Cr-coated Janus colloids, but requires self-propulsion induced by AC electric-field driving.

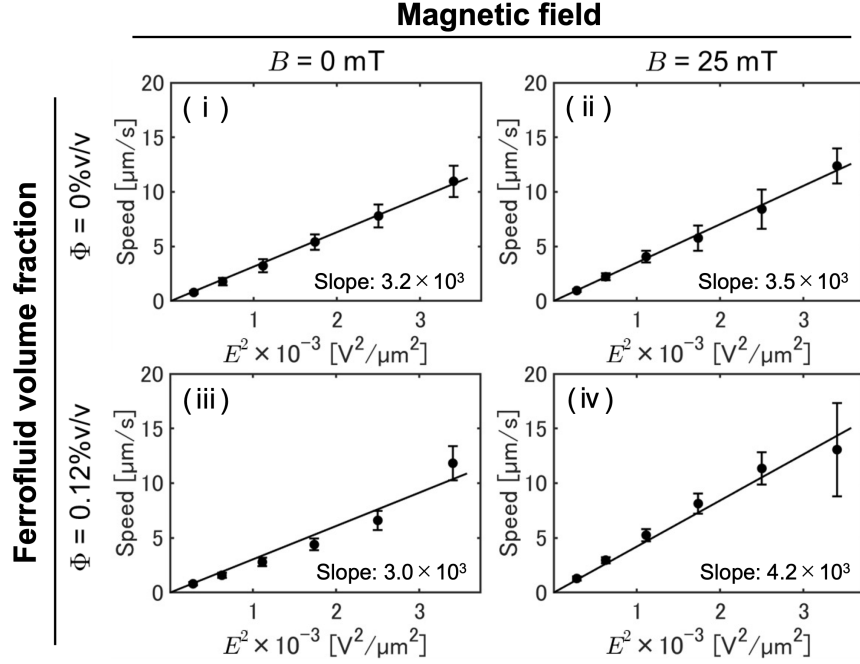


FIG. S3. The propulsion speed of Cr-coated Janus colloids as a function of E^2 . The instantaneous velocity $\mathbf{v} = v\mathbf{p}$ was calculated from the trajectories of active colloids moving in either an aqueous solution ((i), $\Phi = 0\%$, $B = 0$ mT; (ii) $\Phi = 0\%$, $B = 25$ mT, top-right) or a ferrofluid ((iii) $\Phi = 0.12\%$, $B = 0$ mT; (iv) $\Phi = 0.12\%$, $B = 25$ mT). As shown by the fitting curves in each panel, although the slopes slightly differ among the conditions, the mean value of particle speed \bar{v} scales as E^2 . Error bars represent standard deviation.

PROPULSION SPEED OF SELF-PROPELLED JANUS COLLOIDAL PARTICLES

We characterized the self-propelled motion of Cr-coated active Janus colloids by measuring their speed as a function of the applied AC electric field E . The particle position was defined as $\mathbf{r}(t) = (x(t), y(t))$, and the instantaneous velocity as $\mathbf{v}(t) = \dot{\mathbf{r}} = d\mathbf{r}/dt$, estimated from position increments over the time interval of 1.0 s. Using this definition, we compared the particle motility in an aqueous solution ($\Phi = 0\%$ v/v) and in a ferrofluid ($\Phi = 0.12\%$ v/v). For each medium, we further examined both the zero-field condition ($B = 0$ mT) and the field-applied condition ($B = 25$ mT) to test whether the propulsion speed scales with E^2 , as expected for ICEP-driven propulsion. In all cases, the ensemble-averaged propulsion speed \bar{v} was found to scale as E^2 (Fig. S3), indicating that the basic ICEP propulsion mechanism is preserved irrespective of the medium and the magnetic field.

The fitted slope is slightly larger for particles undergoing cross-field motion in the ferrofluid under $B = 25$ mT (0.29) than under the other conditions (0.22–0.24) (Fig. S3). We attribute this difference to the reduced orientational fluctuations in the cross-field state, which promote straighter trajectories and therefore a larger trajectory-based estimate of \bar{v} .

MEAN-SQUARED DISPLACEMENT

We calculated the mean-squared displacement (MSD) of Cr-coated Janus colloids dispersed in an aqueous solution. Both in the presence ($B = 25$ mT) and absence ($B = 0$ mT) of a magnetic field, particles driven at $E = 0.017$ V/ μm exhibit superdiffusive behavior (blue and red curves in Fig. S4).

The MSD, $\langle(\Delta\mathbf{r}(\Delta t))^2\rangle$, is defined as

$$\langle(\Delta\mathbf{r}(t))^2\rangle = \langle[\mathbf{r}(t' + t) - \mathbf{r}(t')]^2\rangle_{t'} \propto t^\alpha, \quad (\text{S1})$$

where $\langle\cdot\rangle_{t'}$ denotes an ensemble average over the time t' .

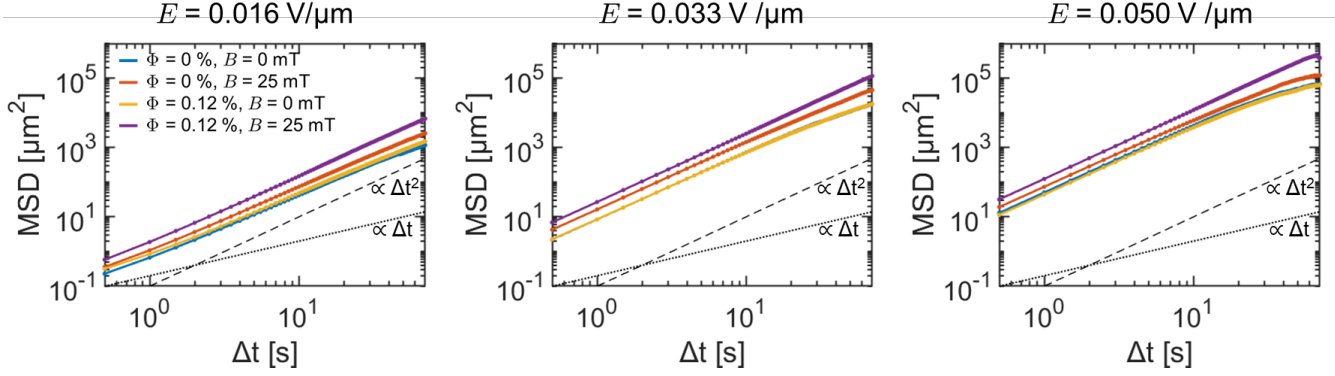


FIG. S4. Mean-squared displacement (MSD) of active Janus colloids in an aqueous solution and ferrofluid under different magnetic-field conditions. MSD data in the range $t = 1\text{--}20\text{ s}$ were fitted to Eq. (S1) to determine the power-law exponent α . The AC electric field driving the motion of the active colloids was varied as $E = 0.017\text{ V}/\mu\text{m}$ (left), $0.033\text{ V}/\mu\text{m}$ (center), and $0.050\text{ V}/\mu\text{m}$ (right). The dashed line indicates ballistic motion ($\text{MSD} \sim t^2$), while the dotted line represents normal diffusion ($\text{MSD} \sim t$). In the aqueous solution without the magnetic field ($\Phi = 0\%$, $B = 0\text{ mT}$), the MSD curves exhibit superdiffusive behavior with scaling exponents $\alpha = 1.80, 1.94,$ and 1.94 for applied AC electric field of $E = 0.017\text{ V}/\mu\text{m}$ (left), $0.033\text{ V}/\mu\text{m}$ (center), and $0.050\text{ V}/\mu\text{m}$ (right), respectively. In the aqueous solution under the magnetic field ($\Phi = 0\%$, $B = 25\text{ mT}$), the MSD scalings are $\alpha = 1.82, 1.95,$ and 1.92 for $E = 0.017\text{ V}/\mu\text{m}$ (left), $0.033\text{ V}/\mu\text{m}$ (center), and $0.050\text{ V}/\mu\text{m}$ (right), respectively, remaining unchanged from the zero-field case. In contrast, in the ferrofluid without the magnetic field ($\Phi = 0.12\%$, $B = 0\text{ mT}$), similar superdiffusive scaling is observed, with $\alpha = 1.72, 1.93,$ and 1.94 at $E = 0.017\text{ V}/\mu\text{m}$ (left), $0.033\text{ V}/\mu\text{m}$ (center), and $0.050\text{ V}/\mu\text{m}$ (right), respectively. In the ferrofluid under a magnetic field ($\Phi = 0.12\%$, $B = 25\text{ mT}$), the MSD approaches ballistic scaling, $\alpha = 1.89, 1.97,$ and 1.98 for $E = 0.017\text{ V}/\mu\text{m}$ (left), $0.033\text{ V}/\mu\text{m}$ (center), and $0.050\text{ V}/\mu\text{m}$ (right), respectively. These scaling exponents reflect the suppression of orientational fluctuations due to cross-field alignment.

At higher driving electric fields ($E = 0.033\text{ V}/\mu\text{m}$ and $E = 0.05\text{ V}/\mu\text{m}$), the magnitude of the MSD increases with E . In contrast, the superdiffusive exponent α remains nearly unchanged regardless of whether the magnetic field is applied. These results show that, in an aqueous solution, the applied magnetic field does not alter the statistics of the self-propelled motion, consistent with the magnetic inertness of the active Janus colloids.

We next examined the MSD in a ferrofluid at a volume fraction of $\Phi = 0.12\%v/v$. In the absence of an applied magnetic field ($B = 0\text{ mT}$), the active colloids still exhibit superdiffusive behavior (yellow curves in Fig. S4), similar to that observed in the aqueous solution. By contrast, in the ferrofluid under a magnetic field of $B = 25\text{ mT}$, the MSD displays nearly ballistic scaling, with exponents $\alpha = 1.89\text{--}1.97$ over all applied AC electric fields (purple curves in Fig. S4). This ballistic behavior arises because the magnetoviscous torque steers particle motion transverse to the magnetic field, thereby maintaining long-lived directional persistence.

CROSS-FIELD MOTION OF AU-COATED JANUS COLLOIDAL PARTICLES

Because Cr-coated Janus colloids do not respond to a magnetic field in the absence of a ferrofluid, the particles themselves are not expected to be directly affected by external magnetic fields with flux densities within $B = 30\text{ mT}$. To examine the dependence on the type of metallic coating, we therefore investigated whether Janus colloids coated with gold (Au) likewise exhibit cross-field motion.

Experiments showed that Au-coated Janus colloids at a density of 0.45 ± 0.07 particles/ $1000\text{ }\mu\text{m}^2$ displayed cross-field motion perpendicular to the applied magnetic field in the ferrofluid of $\Phi = 0.12\%v/v$ (Fig. S5(a)-iv). By contrast, they exhibited isotropic motion both in the absence of the ferrofluid irrespective of the magnetic field (Fig. S5(a)-i and ii), and in the ferrofluid when no magnetic field was applied (Fig. S5(a)-iii). The Au-coated Janus colloids used in this study reached propulsion velocities of $4\text{ }\mu\text{m/s}$ to $5\text{ }\mu\text{m/s}$ under a high applied AC electric field of $0.09\text{ V}/\mu\text{m}$.

We analyzed the speed dependence of the cross-field motion using the orientational order parameter $S(t) = \langle \cos 2(\theta_v^j(t) - \theta_B) \rangle_j$, where $\theta_v^j(t)$ denotes the heading angle of the velocity of the j th particle, $\theta_B = 0$ defines the direction of the applied magnetic field, and $\langle \cdot \rangle_j$ denotes an ensemble average over all tracked particles. As in the case of Cr-coated active colloids (Fig. 2(c) in the main text), The time-averaged orientational order parameter S_0 becomes increasingly negative with increasing propulsion speed for Au-coated active colloids (Fig. S5(b)).

We further examined the response dynamics by applying a step-like magnetic field, switching B from 0 mT to

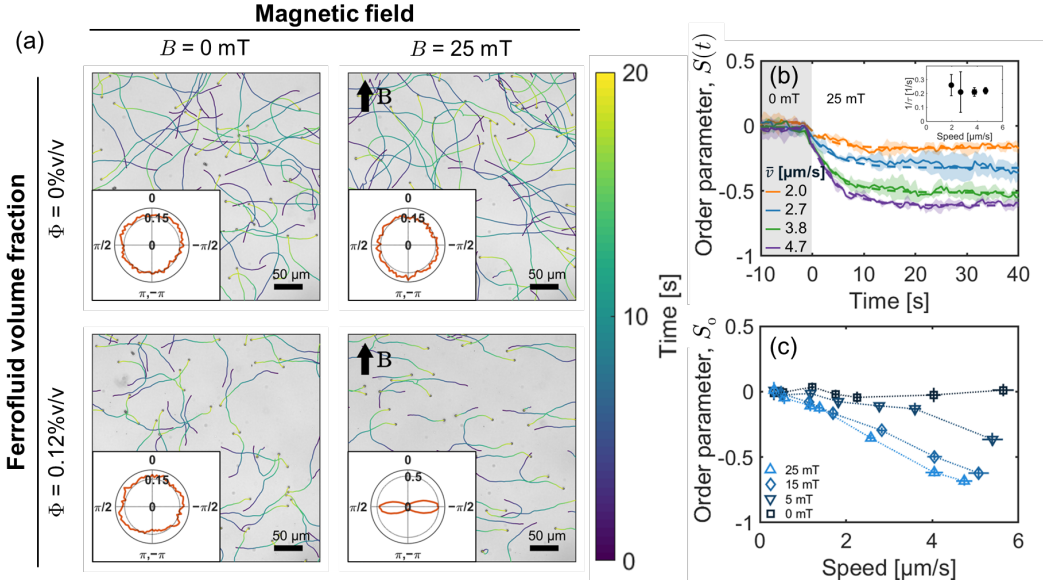


FIG. S5. (a) Cross-field motion of swimming Au-coated Janus colloids in a ferrofluid. Swimming trajectories are color-coded. The uniform magnetic field $B = 25$ mT is applied along the y direction ($\theta = 0$). Inset figure: Probability distribution of the angle of particle swimming. Cross-field motion ($\theta = \pm\pi/2$) is observed in ferrofluids under the applied magnetic field, as in Cr-coated Janus colloids. Scale bar: $50 \mu\text{m}$. (b) The time-averaged orientational order parameter S_0 as a function of the propulsion speed \bar{v} for different magnetic flux densities. (c) Response to the applied magnetic field. At time $t = 0$, the magnetic field is instantaneously switched from $B = 0$ to $B = 25$ mT, and the subsequent time evolution of the orientational order parameter $S(t)$ is analyzed. Inset: Inverse response time, $1/\tau$, as a function of \bar{v} .

15 mT, and analyzing the resulting reorientation rate. Faster-swimming particles responded more rapidly, with the shortest response time being approximately 10 s at $v = 4 - 5 \mu\text{m/s}$ (Fig. S5(c)). This behavior is comparable to that observed for Cr-coated Janus colloids swimming at $v = 4 - 5 \mu\text{m/s}$ (Fig. 2(d) in the main text).

DERIVATION OF CROSS-FIELD MOTION OF A SQUIRMER IN FERROFLUIDS UNDER A UNIFORM MAGNETIC FIELD

We consider a spherical squirmer in a ferrofluid under a uniform magnetic field. A fully self-consistent analytical solution for this system is not readily available. To obtain a tractable description of the leading-order reorientation mechanism, we therefore introduce the following approximations.

First, we assume that the externally applied magnetic field \mathbf{B} is spatially uniform and defines a fixed anisotropy axis

$$\mathbf{e}_B \equiv \mathbf{B}/|\mathbf{B}|.$$

We neglect field-induced spatial restructuring of MNPs, consistent with the observation that the ferrofluid under a magnetic field does not bias the motion of Janus particles under the present experimental conditions (Fig. S2). We instead treat the medium as a homogeneous anisotropic fluid characterized solely by a field-dependent magnetoviscous coefficient η_B . Under these assumptions, the anisotropic stress of ferrofluids $\boldsymbol{\sigma}$ is described by the constitutive form of Mahle *et al.* [44] (Eq. (4) in the main text), in which the field-induced anisotropic stress depends on the local vorticity.

The field-induced stress used in the main text,

$$\boldsymbol{\sigma}_B = \eta_B [\mathbf{e}_B(\mathbf{e}_B \times \boldsymbol{\omega}) - (\mathbf{e}_B \times \boldsymbol{\omega})\mathbf{e}_B], \quad (\text{S2})$$

has an antisymmetric tensor form. This reflects the fact that the magnetoviscous response originates not from ordinary shear deformation, but from a rotational-viscosity mechanism associated with the internal magnetic degrees of freedom of the ferrofluid. In a uniform magnetic field, the magnetic moments of dispersed MNPs tend to align along \mathbf{e}_B . When the surrounding fluid has a local vorticity $\boldsymbol{\omega}$, the flow tends to rotate these moments away from the field direction,

while magnetic torques act to restore the alignment. In linear response, this competition generates a field-dependent internal torque density proportional to $\mathbf{e}_B \times \boldsymbol{\omega}$. In a coarse-grained continuum description, such an internal torque appears as an antisymmetric contribution to the stress tensor, giving rise to the form above Eq. (S2). Thus, the stress $\boldsymbol{\sigma}_B$ should be understood as a rotational-viscosity response arising from the finite relaxation of the magnetization under flow.

Second, following Lintuvuori *et al.* [22], we evaluate the anisotropic stress using the Stokes flow field of a spherical squirmer in an isotropic fluid. In this approximation, the anisotropy enters only through the constitutive law for the stress, while the velocity field itself is taken to be the standard squirmer solution for Stokes flow field. This corresponds to a leading-order treatment in which the feedback effect of the anisotropic viscosity on the flow field is neglected.

With these assumptions, the velocity field of a squirmer is described as [56]

$$\mathbf{u}(\mathbf{r}) = \frac{3}{2}v_0 \left(\frac{a}{r}\right)^2 \left[\frac{a}{r} \left(\frac{2}{3}\mathbf{p} + \sin\vartheta \mathbf{e}_\vartheta \right) + \frac{\beta}{2} \left\{ \left(\frac{a^2}{r^2} - 1 \right) (3\cos^2\vartheta - 1)\mathbf{e}_r + \left(\frac{a}{r} \right)^2 \sin 2\vartheta \mathbf{e}_\vartheta \right\} \right], \quad (\text{S3})$$

where $\mathbf{e}_r = \mathbf{r}/|\mathbf{r}|$ is the radial unit vector and \mathbf{e}_ϑ is the polar unit vector defined with respect to the particle polarity \mathbf{p} . The corresponding vorticity field $\boldsymbol{\omega} \equiv \nabla \times \mathbf{u}$ is

$$\boldsymbol{\omega} = -\frac{9}{2}\beta v_0 \frac{a^2}{r^3} (\mathbf{p} \cdot \hat{\mathbf{r}}) (\mathbf{p} \times \hat{\mathbf{r}}). \quad (\text{S4})$$

The field-induced part of the stress, $\boldsymbol{\sigma}_B$, gives rise to a traction on the particle surface,

$$\mathbf{f}_B = \boldsymbol{\sigma}_B|_{r=a} \cdot \hat{\mathbf{r}} = -\frac{9}{2}\eta_B \frac{\beta v_0}{a} (\mathbf{p} \cdot \hat{\mathbf{r}}) [(\mathbf{p} \cdot \hat{\mathbf{r}})(\mathbf{e}_B \cdot \hat{\mathbf{r}})\mathbf{e}_B - (\mathbf{e}_B \cdot \mathbf{p})\mathbf{e}_B - (\mathbf{e}_B \cdot \hat{\mathbf{r}})^2 \mathbf{p} + (\mathbf{e}_B \cdot \hat{\mathbf{r}})(\mathbf{e}_B \cdot \mathbf{p})\hat{\mathbf{r}}] \quad (\text{S5})$$

with $\eta_B \equiv \frac{\alpha(B)B^2}{4\mu_0}$.

Not surprisingly, the net force vanishes,

$$\mathbf{F}_B = \int_S \mathbf{f}_B dS = \mathbf{0}, \quad (\text{S6})$$

as expected in the absence of an external potential. In contrast, the surface traction is spatially asymmetric and therefore generates a finite torque

$$\mathbf{T} = \int_S a\hat{\mathbf{r}} \times \mathbf{f}_B dS = \frac{6}{5}\pi\eta_B a^2 \beta v_0 (\mathbf{p} \cdot \mathbf{e}_B) (\mathbf{p} \times \mathbf{e}_B) \quad (\text{S7})$$

This result shows that the reorientation torque is proportional to both the swimming strength v_0 and the anisotropic magnetoviscous coefficient η_B .

Assuming overdamped rotational dynamics, the reorientation torque is balanced against the rotational viscous drag $8\pi\eta_0 a^3 \boldsymbol{\Omega}$. We then obtain the angular velocity induced by the anisotropic stress

$$\boldsymbol{\Omega} = \frac{3}{20} \frac{\beta v_0}{a} \frac{\eta_B}{\eta_0} (\mathbf{p} \cdot \mathbf{e}_B) (\mathbf{p} \times \mathbf{e}_B), \quad (\text{S8})$$

We now restrict the motion to the xy plane, consistent with the experimental geometry. We define the polarity angle of the particle orientation θ_p from the magnetic-field axis \mathbf{e}_B , defined as $\theta_p \equiv \cos^{-1}(\mathbf{p} \cdot \mathbf{e}_B)$. The equations of motion then read

$$\dot{x} = v_0 \sin\theta_p, \quad \dot{y} = v_0 \cos\theta_p, \quad \dot{\theta}_p = \Gamma \sin(2\theta_p), \quad (\text{S9})$$

where

$$\Gamma = -\frac{3}{40} \frac{\beta v_0}{a} \frac{\eta_B}{\eta_0}. \quad (\text{S10})$$

For a pusher ($\beta < 0$), $\Gamma > 0$ and the stable orientations are $\theta = \pm\pi/2$, corresponding to cross-field motion.

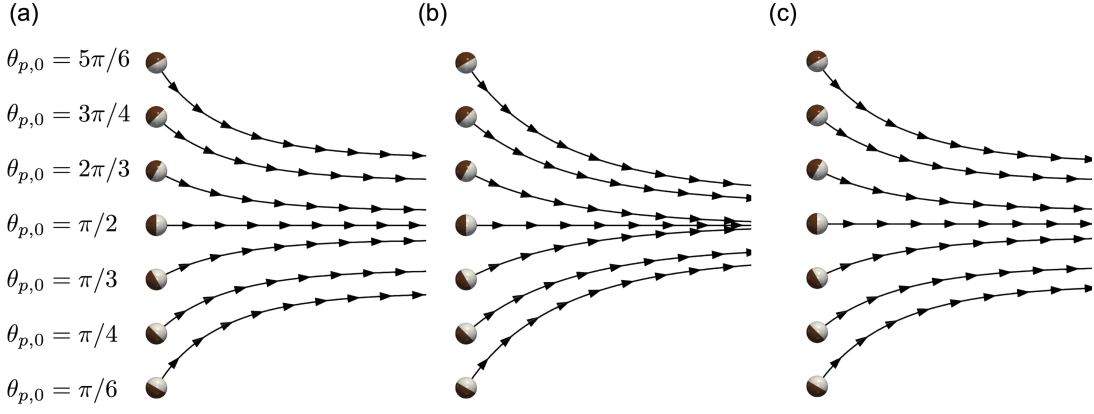


FIG. S6. Cross-field motion of active particles in ferrofluids for $\eta_B/\eta_0 = 0.5$ obtained from analytical solution and direct numerical simulations. (a) Analytical solution for the squirmer model with $\beta = -1$. (b) Direct numerical simulation of the squirmer model with $\beta = -1$. (c) Direct numerical simulation of ICEP-driven active Janus colloids.

Eqns. (S9) can be solved analytically as

$$\begin{aligned}
 x(t) &= \frac{v_0}{4\Gamma} \ln \left[\left| \frac{1 + \sin \theta_p}{1 - \sin \theta_p} \right| \left| \frac{1 - \sin \theta_0}{1 + \sin \theta_0} \right| \right] + x_0 \\
 y(t) &= \frac{v_0}{4\Gamma} \ln \left[\left| \frac{1 - \cos \theta_p}{1 + \cos \theta_p} \right| \left| \frac{1 + \cos \theta_0}{1 - \cos \theta_0} \right| \right] + y_0 \\
 \tan \theta_p(t) &= \tan \theta_0 e^{2\Gamma t}
 \end{aligned} \tag{S11}$$

The trajectories of squirmer particles are shown in Fig. S6(a).

We emphasize that this derivation is intended to isolate the leading-order hydrodynamic mechanism of cross-field motion experimentally observed. In particular, it neglects the feedback of the anisotropic viscosity on the velocity field itself. This higher-order effect may modify quantitative coefficients, but the present minimal treatment captures the directional symmetry breaking of spherical Janus colloids and the dependence of the emergent reorientation torque on both self-propulsive motion (propulsion speed v_0) and anisotropic rheology in bulk fluid (magnetoviscous coefficient η_B) in Eq. (S10).

DIRECT NUMERICAL SIMULATIONS OF AN ICEP JANUS PARTICLE IN FERROFLUIDS

We explicitly solve for an ICEP Janus particle in ferrofluids through direct numerical simulations. To do this, we employ the smoothed profile method [59, 61]. In this method, the sharp boundary between the particle and the surrounding fluid is replaced by a continuous diffuse interface of thickness ξ through a smoothed profile function $\phi \in [0, 1]$, which takes the value $\phi = 1$ inside the particle and $\phi = 0$ in the fluid domain. The mathematical definition of ϕ is given in Ref. [62]. The total velocity $\mathbf{u} = \mathbf{u}_f + \mathbf{u}_p$, consisting of the host fluid \mathbf{u}_f and particle contributions \mathbf{u}_p , evolves according to a modified Navier–Stokes equation,

$$\nabla \cdot \mathbf{u} = 0, \quad \rho(\partial_t + \mathbf{u} \cdot \nabla) \mathbf{u} = \nabla \cdot \boldsymbol{\sigma} + \rho\phi(\mathbf{f}_p + \mathbf{f}_s) \tag{S12}$$

Here, ρ is the fluid density and $\boldsymbol{\sigma}$ is the fluid stress tensor, given by Eq. (4) in the main text. The body force \mathbf{f}_p enforces the rigidity of the particle, whereas \mathbf{f}_s represents the force distribution associated with the prescribed slip-velocity \mathbf{u}^S [60]. This formulation has been successfully applied to non-Newtonian solvents [62, 63]. The translational and rotational motions of the spherical particle are governed by the Newton–Euler equations,

$$\dot{\mathbf{R}} = \mathbf{V}, \tag{S13}$$

$$M\dot{\mathbf{V}} = \mathbf{F}^H + \mathbf{F}^{\text{slip}}, \tag{S14}$$

$$\dot{\mathbf{p}} = \boldsymbol{\Omega} \times \mathbf{p} \tag{S13}$$

$$\mathbf{I} \cdot \dot{\boldsymbol{\Omega}} = \mathbf{T}^H + \mathbf{T}^{\text{slip}} \tag{S14}$$

where \mathbf{R} and \mathbf{V} denote the position and velocity of the particle, respectively, \mathbf{p} is the particle orientation, and $\boldsymbol{\Omega}$ is the angular velocity. \mathbf{F}^H and \mathbf{T}^H are the hydrodynamic force and torque, whereas \mathbf{F}^{slip} and \mathbf{T}^{slip} denote the force and torque arising from the imposed slip motion.

We performed simulations for both a single squirmer, whose slip velocity is given by Eq. (3) in the main text, and an ICEP Janus particle. For the Janus particle, the slip velocity is given by [53, 57],

$$\mathbf{u}^S = \begin{cases} 0 & (0 \leq \vartheta \leq \pi/2) \\ -\frac{9}{8}U_0 (\sin 2\vartheta \cos^2 \varphi \mathbf{e}_\vartheta - \sin \vartheta \sin 2\varphi \mathbf{e}_\varphi) & (\pi/2 < \vartheta \leq \pi). \end{cases} \quad (\text{S15})$$

The particle radius was set to $a = 5\Delta$, and the interface thickness was $\xi = 2\Delta$, where Δ is the grid spacing. The particle was placed in a cubic simulation box of side length $L = 128\Delta$, with periodic boundary conditions imposed in all directions. Previous studies using the smoothed profile method have shown that this particle resolution is sufficient to accurately capture non-Newtonian hydrodynamic effects around squirmers [63].

Both the squirmer slip (Eq. (3) in the main text) and the ICEP slip (Eq. (S15)) yield qualitatively identical reorientation in the simulations (Fig. S6(b) and Fig. S6(c), respectively). Trajectories initialized at various orientations converge to motion transverse to \mathbf{B} . This confirms that the squirmer model captures the essential physics of the Janus ICEP system.

DERIVATION OF THE STEADY-STATE ORIENTATIONAL DISTRIBUTION

The deterministic reorientation dynamics of a squirmer in a ferrofluid is described by Eqs. (S9) and (S10),

$$\dot{\theta}_p = \Gamma \sin(2\theta_p), \quad \Gamma = -\frac{3}{40} \frac{\beta v_0}{a} \frac{\eta_B}{\eta_0}. \quad (\text{S16})$$

In experiments, the particle orientation fluctuates due to rotational noise. We therefore rewrite Eq. (S16) with an additive Gaussian white-noise term $\xi(t)$ and write a Langevin-type equation,

$$\dot{\theta}_p = \Gamma \sin(2\theta_p) + \xi(t). \quad (\text{S17})$$

The noise satisfies $\langle \xi(t) \rangle = 0$ and $\langle \xi(t)\xi(t') \rangle = 2D_\theta \delta(t - t')$, where D_θ is the rotational diffusion coefficient and $\delta(\cdot)$ denotes the Dirac delta function. Eq. (S17) thus describes overdamped angular dynamics in an effective drift field $\Gamma \sin(2\theta_p)$.

The corresponding Fokker–Planck equation for the probability density $P(\theta_p, t)$ follows from the standard expansion as

$$\frac{\partial P(\theta_p, t)}{\partial t} = -\Gamma \frac{\partial}{\partial \theta_p} [(\sin 2\theta_p)P(\theta_p, t)] + D_\theta \frac{\partial^2 P(\theta_p, t)}{\partial \theta_p^2}. \quad (\text{S18})$$

To obtain the steady-state distribution $P(\theta_p)$, we set $\partial_t P(\theta_p, t) = 0$ and impose the condition of vanishing probability flux for a periodic angular variable. This yields

$$\frac{\partial P}{\partial \theta_p} = \frac{\Gamma}{D_\theta} \sin(2\theta_p) P(\theta_p). \quad (\text{S19})$$

Integrating Eq. (S19) gives

$$\ln P(\theta_p) = -\frac{\Gamma}{2D_\theta} \cos(2\theta_p) + \text{const.} \quad (\text{S20})$$

Using $\cos(2\theta) = 2\cos^2\theta - 1$, the constant term can be absorbed into the normalization. We then obtain

$$P(\theta_p) = P_0 \exp\left(-\frac{\Gamma}{D_\theta} \cos^2 \theta_p\right), \quad (\text{S21})$$

which corresponds to Eq. (8) in the main text. The normalization constant P_0 is determined by $\int_0^{2\pi} P(\theta_p) d\theta_p = 1$.

By measuring the orientational angle of active colloids and fitting the resulting distribution with Eq. (S21), the ratio Γ/D_θ can be extracted (Fig. S7(a)). In addition, the rotational diffusion coefficient D_θ is determined independently from the trajectories of active Janus colloids at field-off and torque-free conditions (Fig. S7(b)). Specifically, the autocorrelation function of the swimming direction $\theta_v(t)$ was calculated as $\langle \cos[\theta_v(t' + t) - \theta_v(t')] \rangle_{t'}$ = $\exp(-D_\theta t)$ where t is the time lag. We extracted D_θ from the autocorrelation function calculated for each particle trajectory and then computed the mean value for each speed range. We used their average over all speed ranges, $D_\theta = 0.051 \text{ s}^{-1}$, for the quantitative estimation of Γ .

LINEARIZED RELAXATION DYNAMICS OF THE ORIENTATIONAL ORDER PARAMETER $S(t)$

We show that, in the presence of rotational noise, the order parameter $S(t)$ obeys a single-exponential relaxation equation in the vicinity of the stable orientations. For pushers ($\beta < 0$), one has $\Gamma > 0$, and the stable orientations are $\theta_p = \pm\pi/2$.

To describe the long-time relaxation toward one of these stable states, we expand θ_p as $\theta_p = \pi/2 + \delta\theta_p$, where $\delta\theta_p$ is an infinitesimal deviation under a large reorientation rate ($D_\theta \ll \Gamma$). We then obtain $\sin(2\theta_p) \simeq -2\delta\theta_p$, and Eq. (S17) reduces to the Ornstein–Uhlenbeck form

$$\frac{d\delta\theta_p}{dt} = -2\Gamma\delta\theta_p + \xi(t). \quad (\text{S22})$$

The corresponding equation for the second moment is

$$\frac{d}{dt}\langle(\delta\theta_p)^2\rangle = -4\Gamma\langle(\delta\theta_p)^2\rangle + 2D_\theta. \quad (\text{S23})$$

Next, we relate this fluctuation magnitude to the orientational order parameter

$$S(t) = \langle\cos 2(\theta_p(t) - \theta_B)\rangle. \quad (\text{S24})$$

Here we use the fact that, for the active colloids considered here, the swimming direction θ_v coincides with the angle of the particle polarity vector θ_p (Fig. S1). The direction of the uniform magnetic field is defined as $\theta_B = 0$. The notation $\langle\cdot\rangle$ denotes the ensemble average over the particle population.

Using the expansion $\cos 2\theta_p \simeq -(1 - 2(\delta\theta_p)^2)$, Eq. (S24) becomes

$$S(t) \simeq -1 + 2\langle(\delta\theta_p)^2\rangle. \quad (\text{S25})$$

Substituting Eq. (S23) into the time derivative of Eq. (S25), and eliminating $\langle(\delta\theta_p)^2\rangle$ using Eq. (S25), we arrive at the relaxation equation

$$\frac{dS}{dt} = -4\Gamma(S - S_0), \quad (\text{S26})$$

with the steady-state value $S_0 = -1 + D_\theta/\Gamma$ under the linearized approximation.

We find that Eq. (S26) has the solution

$$S(t) = S_0 + [S(0) - S_0]e^{-4\Gamma t}. \quad (\text{S27})$$

For an initially isotropic state, $S(0) \simeq 0$, this becomes

$$S(t) = S_0 \left(1 - e^{-\frac{t}{\tau}}\right), \quad (\text{S28})$$

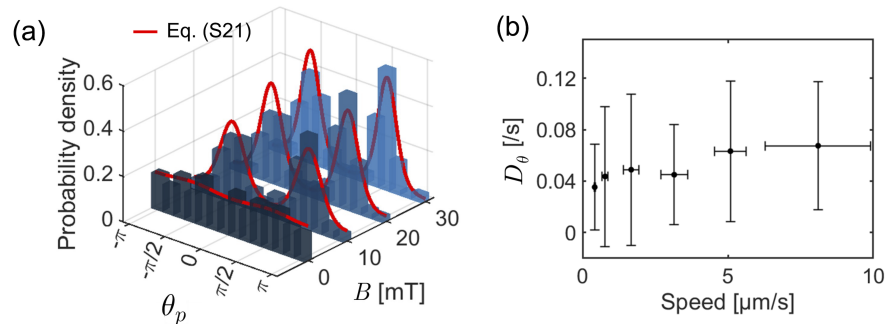


FIG. S7. (a) Probability density of θ_p under various magnetic fields. The range of propulsion speed is $v = 4\text{--}6\ \mu\text{m/s}$. Red line is fit to Eq. (S21). (b) Rotational diffusion constant D_θ as a function of \bar{v} . Error bars represent the standard deviation.

with the characteristic response time

$$\tau = \frac{1}{4\Gamma}. \quad (\text{S29})$$

Thus, in the vicinity of the stable orientations, the noisy orientational dynamics predicts a single-exponential relaxation of the orientational order parameter. Eqs. (S28) and (S29) therefore explains the exponential relaxation in Eq. (2) of the main text.

In addition, using the expression of Γ in Eq. (S10), the steady-state value $S_0 = -1 + D_\theta/\Gamma$ for pushers ($\beta < 0$) can be written as

$$S_0 = -1 + \frac{40a\eta_0 D_\theta}{3|\beta|v_0\eta_B}. \quad (\text{S30})$$

This expression shows that, within the linearized approximation, S_0 approaches -1 as the propulsion speed v_0 or the magnetoviscous coefficient η_B increases, whereas larger rotational diffusion D_θ weakens the alignment. Thus, faster propulsion and stronger anisotropic viscosity can enhance the steady cross-field alignment. Figs. 2(c, d) in the main text also show that the deviation of S_0 from -1 decreases as the propulsion speed \bar{v} increases. This trend is consistent with Eq. (S30).

RAPID AND REVERSIBLE CONTROL OF CROSS-FIELD MOTION OF JANUS COLLOIDAL PARTICLES

To demonstrate reversible control of cross-field motion, we alternately switched the magnetic field on and off at 60 s intervals and quantified the response using the orientational order parameter $S(t)$. Representative microscopy images show isotropic motion in the field-off state and pronounced cross-field motion with the propulsion speed $\bar{v} = 10.5 \mu\text{m/s}$ in the field-applied condition (Fig. S8(a)). The corresponding time trace of $S(t)$ confirms that cross-field alignment is established within 2 s to 3 s after field activation and relaxes back to the isotropic state within a similar timescale after the field is turned off (Fig. S8(b)). This fast on-off response, comparable to the rotational diffusion timescale of the Janus colloids, demonstrates rapid and reversible magnetic control of the swimming direction.

SUPPLEMENTARY MOVIES

- Movie 1: Cross-field motion of active Janus colloids in the ferrofluid under the applied magnetic field, corresponding to the condition (iv) $\Phi = 0.12\%$, $B = 25 \text{ mT}$. The ICEP driving condition is $E = 0.058 \text{ V}/\mu\text{m}$ at 2 kHz. Scale bar is 100 μm .
- Movie 2: Transport of polystyrene cargo particles by an active Janus colloid showing cross-field motion ($\Phi = 0.24\%$, $B = 30 \text{ mT}$). The trajectory of the swimming Janus colloid is color-coded in blue to yellow, and the cargo particles are in white to red. The ICEP driving condition is $E = 0.033 \text{ V}/\mu\text{m}$ at 2 kHz. Scale bar is 10 μm .
- Movie 3: Reversible control of cross-field motion of active Janus colloidal particles. The applied magnetic field is alternately switched on and off at 60 s intervals. Scale bar is 100 μm .

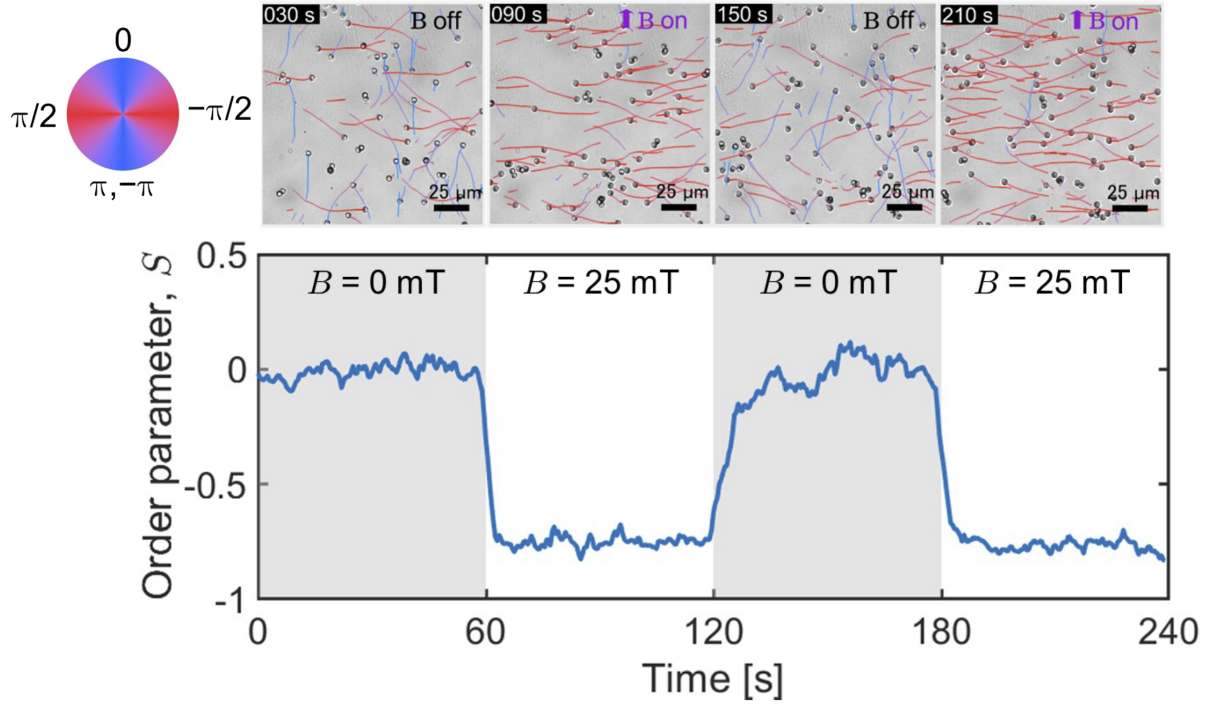


FIG. S8. (a) Reversible switching of cross-field motion induced by turning the magnetic field ($B = 25 \text{ mT}$) on and off. The driving AC field is $E = 0.058 \text{ V}/\mu\text{m}$, and the propulsion speed $\bar{v} = 10.5 \mu\text{m}/\text{s}$. Colored lines in the microscopy images indicate the instantaneous orientation of the particles. The magnetic field is applied along the y direction. Scale bars: $25 \mu\text{m}$. (b) Time evolution of the orientational order parameter $S(t)$. The magnetic field is alternately switched on and off at 60 s intervals. The orientational order parameter alternates between values close to $S = 0$ and $S = -0.8$, and the response time τ is within 2 s to 3 s, demonstrating reversible and repeatable switching of cross-field alignment.